ChemPubSoc Europe

DOI: 10.1002/cssc.201601234

CHEMSUSCHEM Full Papers

The Quest for Value-Added Products from Carbon Dioxide and Water in a Dielectric Barrier Discharge: A Chemical Kinetics Study

Ramses Snoeckx,*[a] Alp Ozkan,[b] Francois Reniers,[b] and Annemie Bogaerts[a]

Recycling of carbon dioxide by its conversion into value-added products has gained significant interest owing to the role it can play for use in an anthropogenic carbon cycle. The combined conversion with H_2O could even mimic the natural photosynthesis process. An interesting gas conversion technique currently being considered in the field of CO_2 conversion is plasma technology. To investigate whether it is also promising for this combined conversion, we performed a series of experiments and developed a chemical kinetics plasma chemistry model for a deeper understanding of the process. The main products formed were the syngas components CO and H_2, as well as O_2 and H_2O_2, whereas methanol formation was only observed in the parts-per-billion to parts-per-million range. The syngas ratio, on the other hand, could easily be controlled by varying both the water content and/or energy input. On the basis of the model, which was validated with experimental results, a chemical kinetics analysis was performed, which allowed the construction and investigation of the different pathways leading to the observed experimental results and which helped to clarify these results. This approach allowed us to evaluate this technology on the basis of its underlying chemistry and to propose solutions on how to further improve the formation of value-added products by using plasma technology.

Introduction

Throughout history the use of natural resources has played a major role in the development of the human race. Among those resources, fossil fuels have contributed to a fast and unprecedented development in human society. However, this has come with a great cost, as burning fossil fuels leads to the emission of large amounts of the greenhouse gas CO_2. Owing to the fact that these anthropogenic CO_2 emissions outpace the natural carbon cycle, the atmospheric CO_2 concentrations have been increasing from 280 ppm since the beginning of the industrial revolution to 400 ppm in 2014.[1] With a high certainty it is this increase that leads to the current adverse global environmental climate changes.[1]

Utilization of this waste (i.e., CO_2) and converting it into a new feedstock (e.g., raw materials for the chemical industry and fuels) not only complies with the framework of sustainable/green chemistry[2,3] but also fits within the "cradle-to-cradle" concept.[4] By generating useful products out of CO_2 we create the possibility to effectively close the carbon loop.

[a] R. Snoeckx, Prof. Dr. A. Bogaerts
Department of Chemistry, research group PLASMANT
University of Antwerp
Universiteitsplein 1, 2610 Antwerp (Belgium)
E-mail: Ramses.snoeckx@uantwerpen.be

[b] A. Ozkan, Prof. Dr. F. Reniers
Chimie analytique et chimie des interfaces
Université Libre de Bruxelles
Campus de la Plaine, Bâtiment A, CP255, boulevard du Triomphe, 1050 Bruxelles (Belgium)

Supporting Information and the ORCID identification number(s) for the author(s) of this article can be found under http://dx.doi.org/10.1002/cssc.201601234.

An interesting co-reactant to pursue this is water. It is not only the most ubiquitous and cheapest hydrogen source, compared to CH_4 and H_2, but in addition, converting CO_2 in combination with H_2O to produce value-added products by using renewable energy would successfully mimic the natural photosynthetic process.[5] Indeed, the successful development of artificial photosynthesis technology is no longer a fairy tale. Furthermore, water is always present in industrial effluent gas streams (fumes). As such, technologies that aim to convert CO_2 immediately at the exit of industrial installations could take advantage of this major and unavoidable "contaminant". Several routes for the combined conversions of CO_2 and H_2O have already reported promising results, for example, thermochemical, electrochemical, and photochemical, either with or without catalysts, and all their possible combinations.[2,6–11] In recent years, another technology considered to have potential in this area is (nonthermal) plasma.[12–14]

The main advantage of (nonthermal) plasma is that the gas can remain near room temperature while being "activated" by electron impact excitation, ionization, and dissociation reactions. Furthermore, nonthermal plasmas do not suffer from the several disadvantages of existing technologies, such as using expensive or scarce materials, the large size of the systems, inefficient energy input for heating of the systems, and short durability of the electrodes. Instead, it is a flexible, so called "turn-key", process operated by a power source and the desired gas mixture, and it can be built with durable inexpensive materials.[15]

Just like electrochemical techniques, plasma technology uses electricity as an energy source. As such, it can also pro-

vide a solution for the imbalance between energy production and consumption by intermittent renewable sources, for example, solar and wind. Taking all the above into account, and especially the fact that plasma is an instantaneous "on-and-off" technique that can use renewable energy sources if they are available, makes plasma an inherent "green" technology. In this scenario, the electrical energy can be stored in a chemical form. The reactions of greatest interest are the conversion of CO_2 into syngas, hydrocarbons, short-chain olefins (i.e., ethylene and propylene), and oxygenated products (i.e. methanol, formaldehyde, dimethyl ether, formic acid, hydrogen peroxide, etc.). For most applications, liquids would be preferable to gases, as they have much higher energy densities (both gravimetric as volumetric) than electrical storage techniques.[16,17] Nevertheless, syngas can easily be converted into almost any commercial bulk chemical or fuel through the Fischer–Tropsch synthesis.[18] For this purpose, it is of great importance to have a high sense of control over the H_2/CO ratio to be able to steer the synthesis towards the desired products.[19]

Other products of interest that can, in principle, be formed starting from CO_2 and H_2O are peroxides. Hydrogen peroxide (H_2O_2) has been shown to be a microbicidal active agent, and its ability to sterilize is widely used and well studied.[20–22] As such, the production of H_2O_2 by plasma technology is gaining a lot of interest for biomedical and (bio-)decontamination applications.[23–25] In a recent extensive review by Lu et al.,[26] which focuses on the generation, transport, and biological effects of the reactive plasma species, H_2O_2 is even considered to be one of the most important reactive oxygen species that acts as a signaling molecule together with O_2^-.

Before explaining the experimental setup and the model, we will give a brief overview on the current state-of-the-art plasma-based combined conversions of CO_2 and H_2O to highlight the main trends observed until now and also to identify the current knowledge gap with respect to the underlying mechanisms. This work aims to fill this knowledge gap by a combination of experiments and especially computations.

State-of-the-art plasma-based combined CO_2 and H_2O conversions

Because of its advantages over conventional reforming technologies, a lot of research has already been devoted to the plasma-based conversion of greenhouse gases into value-added products. Most of the research has been based on pure CO_2 splitting[27–36] or dry reforming of methane.[12,14,37–50] Pure H_2O plasmas for the production of hydrogen have also been extensively studied.[51–55] However, research on the simultaneous conversions of CO_2 and H_2O into syngas or oxygenated products by plasma is very limited. Ihara et al.[56,57] were the first to investigate the conversions of CO_2 and H_2O by means of a microwave plasma setup. Other researchers have considered a ferroelectric packed-bed reactor,[58] a dielectric barrier discharge (DBD),[58] a DBD packed with a Ni/γ-Al_2O_3 catalyst,[59] a surface discharge,[60] a negative direct current (DC) corona discharge,[61] and a surface-wave microwave discharge.[15]

In general, five main trends can be distinguished from the above literature: one, the CO_2 conversion increases with increasing energy input; two, the H_2/CO ratio decreases with increasing energy input; three, the CO_2 conversion decreases with increasing water content; four, the H_2/CO ratio increases with increasing water content; five, the main products formed are H_2, CO, and O_2, but some papers also report the production of hydrogen peroxide (H_2O_2),[56] oxalic acid ($C_2H_2O_4$),[56] formic acid (CH_2O_2),[60] methane (CH_4),[59,60] dimethyl ether (C_2H_6O, DME),[60] methanol (CH_3OH),[57,59,61] and ethanol (C_2H_5OH).[61] Unfortunately, most data on the formation of these products are only qualitative and incomplete, and this makes the deduction of a general trend on product yields or selectivities impossible.

It becomes clear that not much is known about the simultaneous conversions of CO_2 and H_2O into value-added products and, specifically, not much is known about the underlying mechanisms. In this paper, we study the combined plasma-based conversions of CO_2 and H_2O for a DBD plasma reactor by means of experiments and computer simulations on the basis of a zero-dimensional (0D) chemical kinetics model.

The main aim of this study is to evaluate whether the combined conversions of CO_2 and H_2O by using plasma can become a viable route to produce value-added chemicals by identifying and analyzing the underlying plasma chemical kinetic behavior. For this analysis, first a plasma chemical kinetics model for CO_2/H_2O and its interactions needs to be developed. The investigation will then be performed in a stepwise manner by first determining the influence of the water content and the specific energy input (SEI) on the conversion and product formation in a combined effort of experiments and computations. The latter also allows the model to be validated. Subsequently, a detailed chemical kinetics analysis will be performed to elucidate the mechanisms behind the observed trends. This approach enables us to investigate the current and future possibilities and limitations in more detail. Furthermore, on the basis of this analysis we can also suggest possible solutions to enhance the formation of the desired products and, as such, make an initial evaluation towards the industrial viability of plasma technology for this process.

Results and Discussion

First we will compare the measured conversions of CO_2 and H_2O and the product selectivities with the model calculations. We will also discuss in detail the underlying chemistry for the obtained results, on the basis of the model predictions, to explain the observed trends. Subsequently, we will briefly discuss additional simulations for a broader range of conditions to predict the CO_2 and H_2O conversions and the product selectivities at larger SEI values and water contents. Finally, on the basis of this plasma chemical kinetic analysis, we will summarize the current potential and limitations of plasma technology for the combined conversions of CO_2 and H_2O into value-added chemicals and propose some solutions on how to move forward in this field.

Conversion and selectivity: A comparison between experiments and model calculations

CO_2 and H_2O conversion

In Figure 1, the experimental and calculated absolute CO_2 and H_2O conversions are plotted as a function of water vapor content for a total gas flow rate of 600 mL min^{-1} at 323 K for three different SEI values, that is, 3.2, 4.0, and 4.8 J cm^{-3}. As to be expected, the absolute CO_2 and H_2O conversions increase if more energy is supplied, that is, at higher SEI values. Regardless of the SEI, both the experimental and calculated absolute CO_2 conversions are the highest for pure CO_2 if no water vapor is added to the discharge. The experimental conversions in this case are 4.3, 3.3, and 2.6% for the three different SEI values investigated, and the calculated values are very similar.

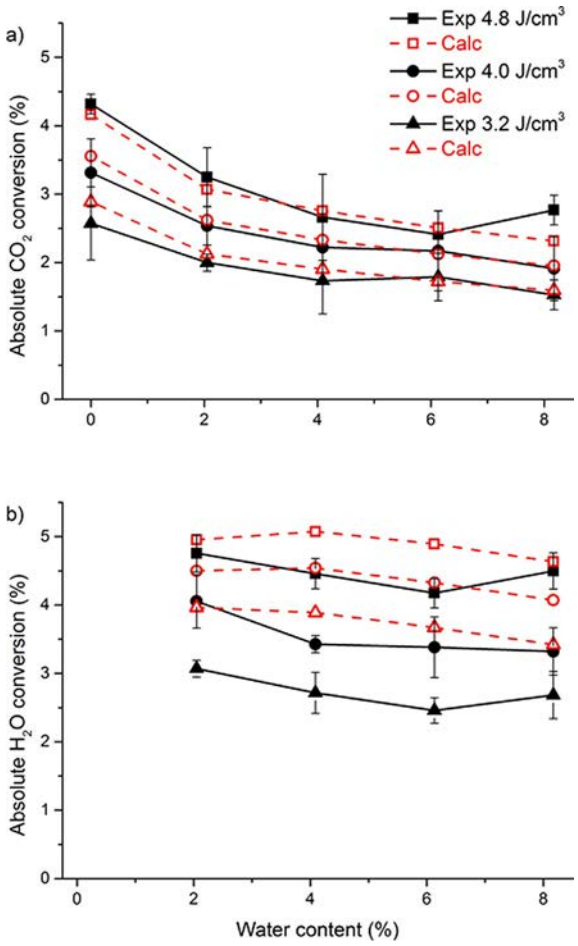

Figure 1. Experimental and calculated values of absolute a) CO_2 and b) H_2O conversion as a function of water vapor content for the different values of SEI and a total flow rate of 600 mL min^{-1} at 323 K.

The drop in CO_2 conversion with increasing water content may result from destabilization of the discharge induced by the presence of water. Indeed, our calculations reveal a drop of approximately 40% in the maximum electron density upon increasing the water content from 0 to 8%. Furthermore, our chemical analysis pathway also allows us to identify a chemical reason for the drop in CO_2 conversion, as will be explained in the underlying mechanism section below. Adding 2% water vapor yields a drop in the CO_2 conversion by approximately 25% for all SEI values investigated. Upon increasing the water content up to 8%, the CO_2 conversion continues to drop slightly by an additional 15–25%, compared to the conversion at 2% water and depending on the SEI. As the CO_2 content in the gas flow drops upon increasing the H_2O fraction, the effective CO_2 conversion will drop even more than the absolute CO_2 conversion, that is, from 4.3–2.6% (depending on the SEI, see above) for pure CO_2, till 2.5–1.4% for 8% H_2O addition (see Figure S3 in the Supporting Information).

The absolute H_2O conversion shows a slightly decreasing trend of approximately 10% upon increasing the water content from 2 to 8%. At a water content of 2%, the absolute experimental H_2O conversions are 4.8, 4.1, and 3.1% for SEI values of 4.8, 4.0, and 3.2 J cm^{-3}, respectively, whereas these values amount to 4.5, 3.3, and 2.7% at a water content of 8%. As the drop in absolute H_2O conversion is limited, the effective H_2O conversion clearly rises at higher water contents (from 2 to 8%), that is, from 0.10 to 0.37%, from 0.08 to 0.27%, and from 0.06 to 0.22% for SEI values of 4.8, 4.0, and 3.2 J cm^{-3}, respectively (see Figure S3).

The calculated H_2O conversions are overestimated, on average by approximately 9.5, 23.5, and 37.3% over the entire range of water addition, for the SEI values of 4.8, 4.0, and 3.2 J cm^{-3}, respectively, relative to the experimental values. This overestimation is probably due to some more complex processes taking place in the experiments as a result of water vapor, which could not be easily accounted for in the 0D plasma chemistry model. Indeed, the model describes all chemical processes, but does not take into account some physical effects, such as condensation and nebulization. It is well possible that evaporation in reality is not complete, and this leads to small droplets (nebulization) of water spread throughout the discharge zone, despite the fact that the entire plasma system is heated starting from the controlled evaporator mixer (CEM). This would lead to a lower concentration of gaseous H_2O that could undergo reactions in the plasma, but nevertheless, this H_2O will also reach the MS capillary and will, thus, be accounted for upon calculating the conversion [see Equation (2)]. Hence, this results in a lower experimental conversion. Upon increasing the SEI, more energy is supplied to the gas and slightly more heat is locally generated in the discharge filaments, which might reduce the probability of condensation, and this may explain the lower deviation between the calculated and measured conversions with increasing SEI values.

Product selectivity

CO_2 splitting typically yields CO and O_2 molecules, the latter of which is formed by the recombination of O atoms. Besides, some O_3 can also be created.[28] Upon the addition of a H source, such as CH_4 or H_2O, we target the production of small oxygenated hydrocarbons, such as formaldehyde, methanol, and formic acid. In the case of CH_4 addition in the plasma, we mainly form syngas, as demonstrated before.[62] In the present

paper, we investigate whether H_2O addition to a DBD plasma can result in some oxygenated molecules, similar to that reported for microwave, atmospheric surface, and negative DC corona discharge plasmas[56,57,60,61] (see above). Unfortunately, for all investigated cases in both the experiments and calculations the main products formed are O_2 and the syngas components CO and H_2. We do form some hydrogen peroxide (H_2O_2) and trace amounts of ozone (O_3), but no oxygenated hydrocarbons are detected in the experiments, and the calculated concentrations of methanol and formaldehyde are only in the parts-per-billion range (hence, far below the experimental detection level). The reason for this will be discussed in more detail in the next section by elucidating the underlying chemistry.

Figure 2 represents the calculated number densities of the most important molecules present or formed in the plasma as a function of time for a SEI of 4 J cm^{-3} and a water content of 4%. The total residence time of the gas in the plasma reactor corresponds to 1.66 s, as indicated above. The CO_2 and H_2O densities show a slightly decreasing trend, in line with their conversions. As a consequence, the main products formed, that is, CO, O_2, and H_2 (and O_3), exhibit the opposite increasing trend, with final concentrations in the percentage range (see also below). H_2O_2 is characterized by a slightly different, more flat trend, and the final concentration is in the parts-per-million range. Finally, the oxygenated products (i.e., CH_2O and CH_3OH), together with CH_4, reach concentrations well below the parts-per-million range.

The measured and calculated concentrations of O_2, CO, H_2, H_2O_2, and O_3 are listed in Table 1 for the different water vapor contents investigated and for a SEI of 4.0 J cm^{-3}. The results for the other SEI values can be found in the Supporting Information.

The agreement between the measured and calculated gas compositions is very good. CO is the main product, as expected (due to the higher CO_2 content in the mixture), but its fraction clearly drops upon increasing the H_2O content, as is also the case for the O_2 and O_3 fractions. The H_2 and H_2O_2 fractions, on the other hand, increase upon adding more H_2O, which is also logical. The O_3 and H_2O_2 contents could—although detectable—not be quantified owing to their low signal-to-noise ratios, so only an order of magnitude could be given for the experimental data in Table 1.

If we take a look at the experimental and calculated H_2/CO ratio (also known as syngas ratio) in Figure 3, we can draw the following conclusions. First, the calculated ratios are higher than the experimental values. This is of course a direct result of the abovementioned overestimation of the H_2O conversion, which leads to a higher concentration of H_2. Second, the SEI has only a minor effect on the syngas ratio in the investigated range. Finally, and most importantly, the H_2/CO ratio increases linearly with increasing water content. This is logical, because

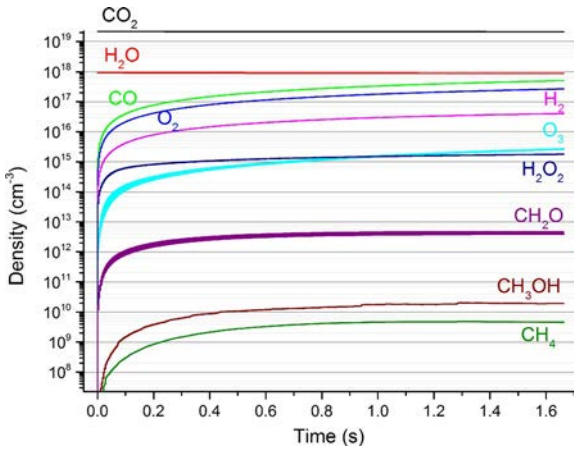

Figure 2. Calculated species densities of the most important molecules present or formed in the plasma as a function of time for a SEI of 4 J cm^{-3} and a water content of 4%.

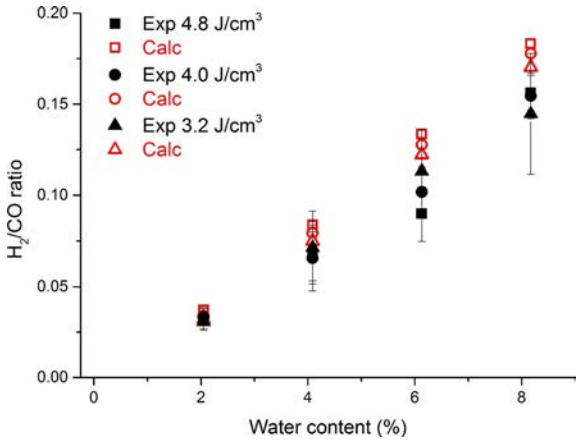

Figure 3. Experimental and calculated values of the H_2/CO ratio as a function of water vapor content for the different values of SEI and a total flow rate of 600 mL min^{-1} at 323 K.

Table 1. Measured and calculated gas compositions after plasma treatment for a SEI of 4.0 J cm^{-3} and for the different water vapor contents investigated with the remainder being unconverted CO_2 and H_2O.

Water content [%]	O_2 [%]	CO [%]	H_2 [%]	H_2O_2 [ppm]	O_3 [ppm]
2.05 (exptl)	1.27 ± 0.11	2.46 ± 0.32	0.081 ± 0.006	10–100	10
2.05 (calcd)	1.28	2.53	0.09	47	193
4.09 (exptl)	1.12 ± 0.18	2.11 ± 0.53	0.138 ± 0.015	10–100	10
4.09 (calcd)	1.17	2.21	0.18	77	118
6.13 (exptl)	1.11 ± 0.13	2.02 ± 0.27	0.205 ± 0.005	10–100	10
6.13 (calcd)	1.09	1.97	0.25	106	96
8.17 (exptl)	1.00 ± 0.08	1.74 ± 0.14	0.269 ± 0.003	10–100	10
8.17 (calcd)	1.03	1.77	0.32	135	81

the absolute H_2O and CO_2 conversions only decrease slightly upon increasing the water content (see above), so a higher water content (and thus a lower CO_2 content) leads to an increase in the effective production of H_2 (formed out of H_2O) and a drop in the CO production (formed out of CO_2). As such, although no detectable amounts of oxygenated hydrocarbons are produced, this type of combined CO_2 and H_2O plasma conversion could still be of significant interest, because changing the water content in the gas mixture allows for a process with an easily controllable H_2/CO ratio. This is very important, as several postprocesses require a different syngas ratio depending on the targeted products.[19] For example, Fischer–Tropsch synthesis needs a ratio of 1.7 or 2.15, depending on the catalyst used, whereas methanol synthesis needs a ratio of 3. The values obtained here, that is, for water vapor contents up to 8%, lead to syngas ratios clearly below 1, and thus, they will need hydrogen enrichment for most practical applications. However, further in this paper we will investigate the conversion process over a wider range of water vapor contents and SEI values, which yield significantly larger syngas ratios up to 8.6 (see below).

Figure 4 illustrates the measured and calculated O-based selectivities of CO and O_2 and the H-based selectivities of H_2 and H_2O_2 as a function of the water vapor content. The results are only shown for a SEI of 3.2 J cm^{-3}, as the absolute values and especially the trends of the selectivities appear to be almost independent of the used SEI; data at other SEI values can be found in the Supporting Information.

The O-based selectivity in Figure 4a indicates that upon increasing the water content from 2 to 8%, the experimental O_2 selectivity increases from 50.3 to 53.2% and the CO selectivity decreases from 48.7 to 46%. The calculated values are in excellent agreement with the measured values (note the detailed *y* axis). The increase in the O_2 selectivity upon increasing the water content can easily be explained by the conversion of H_2O, which leads to the additional formation of O_2 and thus increased selectivity for O_2 and decreased selectivity for CO. The sum of the CO and O_2 selectivities is approximately 99%. The remaining 1% selectivity in both the experimental and calculated results is accounted for by O_3 and H_2O_2.

Figure 4b shows the H-based selectivity versus the water content. The calculated H_2 selectivity is approximately 95–96% and the remaining 4–5% is due to the selectivity towards H_2O_2, independent of the water content within the investigated range. Although it is clear from the MS spectra that H_2O_2 is present in the mixture, its signal-to-noise ratio is too low to quantify exactly its effective amount and, hence, to calculate its selectivity directly. Nevertheless, from the spectra it is possible to estimate its concentration to be in the order of 10–100 ppm. Given that the calculated selectivity for H_2O_2 corresponds to a concentration between 47 and 135 ppm (see Table 1), this is indeed in the same range as the measured values. We calculated the experimental selectivity for H_2 and H_2O_2 for the 10–100 ppm range by taking these values as lower and upper limits, respectively; see shaded area in Figure 4b. As expected, for low water contents the calculated results are closer to the values for 10 ppm, whereas for higher water contents the values are closer to the values of 100 ppm, as our calculations predict an increase in H_2O_2 upon increasing the water content. From these results we may conclude that all calculated selectivity results are in good agreement with the experiments.

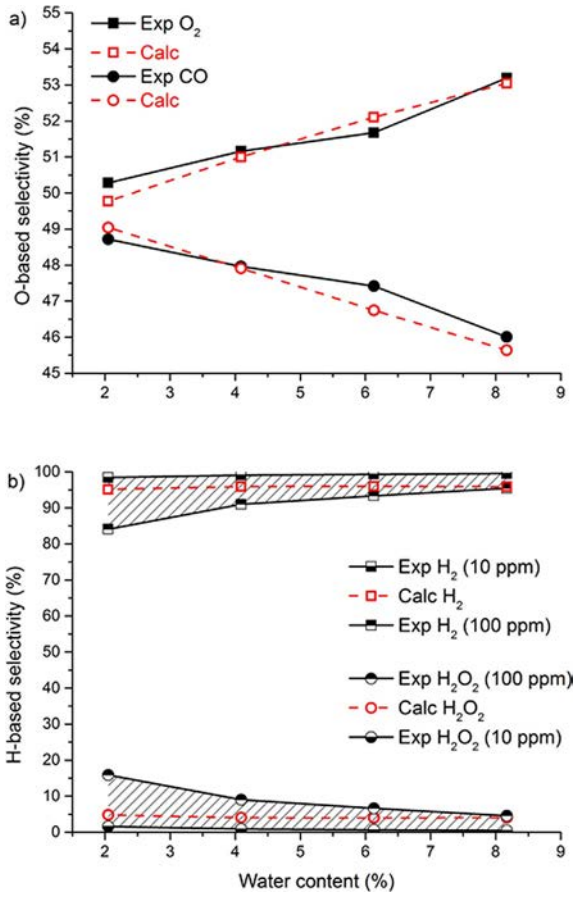

Figure 4. Experimental and calculated values of a) O-based and b) H-based selectivities of the major products as a function of water vapor content for a SEI value of 3.2 J cm^{-3} and a total flow rate of 600 mL min^{-1} at 323 K. Note that although H_2O_2 was detected during the measurements (≈10–100 ppm), it could not be exactly quantified owing to its low signal-to-noise ratio; therefore, a selectivity range is presented for the experimental H-based selectivities.

Energy efficiency

Given that the main products are CO, O_2, and H_2, the energy efficiency can be based on the standard reaction enthalpies (ΔH^0_r)of the following two splitting reactions [Eqs. (1) and (2)]:

$$CO_{2(g)} \rightarrow CO_{(g)} + {}^1/_2\, O_{2(g)} \qquad \Delta H^0_r = 283\ \text{kJ mol}^{-1} \tag{1}$$

$$H_2O_{(g)} \rightarrow H_{2(g)} + {}^1/_2\, O_{2(g)} \qquad \Delta H^0_r = 242\ \text{kJ mol}^{-1} \tag{2}$$

Or combined [Eq. (3)]:

$$CO_{2(g)} + H_2O_{(g)} \rightarrow CO_{(g)} + O_{2(g)} + H_{2(g)} \qquad \Delta H^0_r = 525\ \text{kJ mol}^{-1} \tag{3}$$

As such, we can calculate the energy efficiency (η) for our process by the following formula [Eq. (4)]:

$$\eta = \frac{X_{\mathrm{eff,CO_2}} \cdot 283\ [\mathrm{kJ\,mol^{-1}}] + X_{\mathrm{eff,H_2O}} \cdot 242\ [\mathrm{kJ\,mol^{-1}}]}{\mathrm{SEI}\ [\mathrm{kJ\,mol^{-1}}]} \quad (4)$$

in which X_{eff} is the effective conversion.

The values for the energy efficiencies obtained in this way, both by experiment and calculations, are presented in Table 2.

Table 2. Experimental and calculated energy efficiencies based on the standard reaction enthalpy for the different specific energy inputs and water vapor contents investigated.

SEI [J cm^{-3}]	Water content [%]	η (exptl) [%]	η (calcd) [%]
3.2	2.05	6.7	7.2
	4.09	5.9	6.5
	6.13	6.0	6.0
	8.17	5.3	5.7
4.0	2.05	6.8	7.1
	4.09	6.0	6.4
	6.13	5.9	5.9
	8.17	5.3	5.5
4.08	2.05	7.3	6.9
	4.09	6.0	6.3
	6.13	5.5	5.8
	8.17	6.4	5.5

For pure CO_2 splitting, the thermal equilibrium dissociation limit lies at approximately 60% energy efficiency, and the same target is assumed for the dry reforming of methane.[62–64] At the same time, the energy efficiency of water splitting by electrolysis lies in the same 60–70% range. Therefore, we believe that the same 60% energy efficiency should be the target for the combined process under study here. If we do not take the energy required for evaporating the water and heating the system into account, the highest (measured) energy efficiency achieved in our study is 7.3% for a SEI of 4.8 J cm^{-3} and a water content of 2.05%. As such, it becomes clear that from an energetic point of view the process needs to be improved by at least a factor 8 to be considered competitive. It should be realized, however, that by adding a catalyst, which we believe is necessary to target the production of value-added compounds such as methanol, the energy efficiency of a DBD plasma reactor typically also improves. In most cases, the catalyst is added as beads or pellets in a DBD reactor to yield a so-called packed-bed DBD; this gives rise to electric field enhancements near the contact points of the beads or pellets[65] and leads to higher electron energies and, thus, more pronounced electron impact dissociation of the gas molecules for the same applied power, which results in better energy efficiency. The latter was indeed demonstrated in several papers for pure CO_2 splitting,[66–68] and we believe that similar improvements in energy efficiency would also be possible for combined CO_2/H_2O conversion.

Underlying mechanisms for the observed trends

As shown above, the experiments and computer simulations reveal exactly the same trends for the absolute conversions of CO_2 and H_2O and for the selectivities towards CO, H_2, and O_2. This justifies the use of the plasma chemistry model for the most important—and chemically most interesting part—of this work, that is, analyzing the main reactions taking place to describe and explain the observed macroscopic trends and, eventually, to compile a general reaction scheme that illustrates the overall underlying chemical reaction mechanisms. This allows us in the end to draw important conclusions regarding the applicability of this process.

Limited CO_2 (and H_2O) conversion upon water addition

There are two main reasons why the CO_2 conversion decreases upon adding water: a physical reason and a chemical reason. The physical reason was already mentioned above, namely, the drop in maximum electron density, which leads to a lower rate of the electron impact dissociation reactions. The chemical reason behind the drop in CO_2 conversion upon increasing the water vapor content is revealed by kinetic analysis. One of the crucial reactions for this process is the reaction between CO and OH [Eq. (5)]:

$$\mathrm{CO + OH \rightarrow CO_2 + H} \qquad k = 5.4 \times 10^{-14}\ [\mathrm{cm^3\,molecule^{-1}\,s^{-1}}]\ (T/298\,\mathrm{K})^{1.50}\ \mathrm{e}^{250[\mathrm{K}]/T} \quad (5)$$

This is a fast reaction and plays a pivotal role in the ratio between the conversions of CO_2 and H_2O. We can explain this in a very simple way by means of the following reaction paths that take place:

$$\mathrm{e^- + CO_2 \rightarrow CO + O + e^-} \quad (6)$$

$$\mathrm{e^- + H_2O \rightarrow OH + H + e^-} \quad (7)$$

$$\mathrm{CO + OH \rightarrow CO_2 + H} \quad (8)$$

$$\mathrm{H + O_2 + M \rightarrow HO_2 + M} \quad (9)$$

$$\mathrm{HO_2 + O \rightarrow OH + O_2} \quad (10)$$

$$\mathrm{OH + H + M \rightarrow H_2O + M} \quad (11)$$

Overall reaction:

$$\mathrm{2\,e^- + CO_2 + H_2O \rightarrow CO_2 + H_2O + 2\,e^-} \quad (12)$$

Reactions (6) and (7) lead to the (electron impact) dissociation of CO_2 and H_2O, which yields the products CO and OH (as well as O and H atoms). However, owing to the large reaction rate constant of Reaction (8), CO and OH will quickly recombine to form CO_2 again. In these three reactions, two H atoms and one O atom are formed, but they recombine quickly as well, first into OH through the Reactions (9) and (10), and subsequently, OH reacts even faster with H back into H_2O through Reaction (11). In the end, this leaves us exactly where we start-

ed [see overall Reaction (12)]. Of course, this does not mean that there will be no net conversion of CO_2 and H_2O. Indeed, this is not the only pathway taking place for the conversion of CO_2 and H_2O, but this pathway highlights the interaction between the CO_2 and H_2O dissociation products, which limits their conversion. The overall CO_2 and H_2O loss rates, however, are higher than their formation rates, which effectively leads to the observed conversions. Nevertheless, Reactions (7) and (8) illustrate why the absolute conversion of CO_2 decreases upon adding H_2O, whereas in general an increasing trend is found for the absolute CO_2 conversion in admixtures, that is, upon adding N_2,[69] He,[70,71] and Ar.[71]

Absence of methanol production

The above reaction scheme can also explain why no production of methanol is observed. Indeed, in 1998 Eliasson et al.[72] investigated the production of methanol in a CO_2/H_2 DBD reactor. Upon using the plasma-only setup, the CO_2 conversion reached 12.4% and the major products were CO (with a selectivity of 96%) and H_2O, whereas very low yields of CH_4 and methanol were detected with selectivities of 3.2 and 0.4%, respectively. The authors proposed the following radical reaction mechanism for the formation of methanol [Eq. (13)]:

$$CO_2 \xrightarrow{+e^-} CO \xrightarrow{+H} CHO \xrightarrow{+H} CH_2O \xrightarrow{+H} CH_3O \xrightarrow{+H} CH_3OH \quad (13)$$

These reactions are also included in our model, but they seem to be of minor importance if using H_2O as a co-reactant, because the H atoms are quickly consumed by O_2 and OH, according to the scheme presented above [Reactions (9) and (11)]. Our plasma chemistry model elucidates that in the case of a CO_2/H_2O mixture another pathway to methanol is more important (note that the reactant "+H" above the arrows does not only designate H atoms but can also be replaced by other H-containing species such as H_2, HO_2, H_2O, …) [Eq. (14)]:

$$CO_2(\xrightarrow{+e^-} CO) \xrightarrow{+e^-} C \xrightarrow{+H} CH \xrightarrow{+H} CH_2 \xrightarrow{+H} CH_3 \xrightarrow{+OH} CH_3OH \quad (14)$$

Nevertheless, both these pathways turn out to be unimportant in our case, because the H atoms that are needed to start forming CHO and CH fragments from CO and C, respectively, are steered to OH and subsequently to H_2O again [see Reactions (9)–(11) above], which leaves no room for the production of oxygenated hydrocarbons, such as methanol. This chemical analysis reveals that H_2O might not be a suitable H source for the formation of methanol (as well as other oxygenated hydrocarbons) after all, because of the abundance of O atoms, O_2 molecules, and OH radicals trapping the H atoms. This important new insight will allow us to propose solutions on how the production of methanol might still be pursued in a CO_2/H_2O plasma and/or which other options might be more attractive, as will be elaborated in the summary below.

Formation of H_2O_2

Both our experiments and calculations illustrate that a mixture of CO_2 and H_2O can yield non-negligible amounts of H_2O_2, which is also of great value, more specifically for decontamination purposes, as explained in the Introduction. The main pathways for the production of H_2O_2, as revealed by our chemical kinetics analysis, are [Eqs. (7), (15) and (16)]:

$$2 \times (e^- + H_2O \rightarrow OH + H + e^-) \quad (7)$$

$$OH + OH + M \rightarrow H_2O_2 + M \quad (15)$$

Overall reaction:

$$2\,e^- + 2\,H_2O \rightarrow H_2O_2 + 2\,H + 2\,e^- \quad (16)$$

Reaction (7) leads to the (electron impact) dissociation of H_2O into H and OH. Subsequently, 2 OH radicals react with each other in the presence of a third body to form H_2O_2 [Reaction (15)]. For the operating conditions investigated here, that is, water contents up to 8% and SEI values up to 4.8 $J\,cm^{-13}$, this pathway is responsible for 90% of the production of H_2O_2. The remaining 10% follows a slightly more complicated pathway:

$$3 \times (e^- + CO_2 \rightarrow CO + O + e^-) \quad (6)$$

$$e^- + H_2O \rightarrow OH + H + e^- \quad (7)$$

$$OH + O \rightarrow H + O_2 \quad (17)$$

$$H + O_2 + M \rightarrow HO_2 + M \quad (9)$$

$$HO_2 + O \rightarrow OH + O_2 \quad (10)$$

$$OH + O \rightarrow H + O_2 \quad (17)$$

$$2 \times (H + O_2 + M \rightarrow HO_2 + M) \quad (9)$$

$$HO_2 + HO_2 + M \rightarrow H_2O_2 + O_2 + M \quad (18)$$

Overall reaction:

$$4\,e^- + H_2O + 3\,CO_2 \rightarrow H_2O_2 + 3\,CO + O_2 + 4\,e^- \quad (19)$$

Reactions (6) and (7) again lead to the (electron impact) dissociation of CO_2 and H_2O, which produces CO, O, OH, and H. OH and O subsequently form H and O_2 [Reaction (17)], which then react further with a third body to HO_2 [Reaction (9)]. HO_2 turns out to be the main production source for O_2 and the second most important source for OH [Reaction (10)]. Next, Reactions (17) and (9) can repeat themselves finally to yield two HO_2 radicals, which react with each other in a three-body reaction to produce H_2O_2 and O_2 [Reaction (18)]. Thus, the overall reaction is given by Reaction (19).

General reaction overview

A general reaction overview is illustrated in Figure 5, which is composed of the time-integrated formation and loss rates of

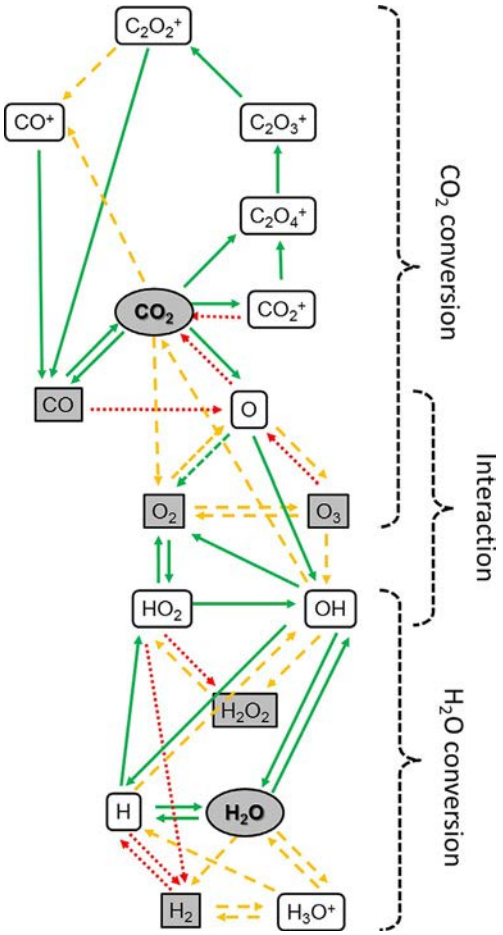

Figure 5. Reaction scheme to illustrate the main pathways for the conversions of CO_2 and H_2O and their interactions. The arrowed lines represent the formation rates of the species, the full green lines are the formation rates over 10^{17} $cm^{-3}s^{-1}$, the orange dashed lines are the formation rates between 10^{17} and 10^{16} $cm^{-3}s^{-1}$, and the red dotted lines are the formation rates between 10^{16} and 10^{15} $cm^{-3}s^{-1}$.

the most important species in our model for explaining the chemical pathways taking place. The results are presented for a SEI of 3.2 $J\,cm^{-3}$ and a water content of 8%. A higher SEI yields higher integrated rates but does not change the reaction paths significantly. A lower water content only decreases the reaction rates of the H_2O chemistry, but again, it does not change the reaction paths significantly.

The reaction scheme can be divided into three main parts: the top part describes CO_2 conversion, the bottom part deals with H_2O conversion, and the middle part explains the interaction between both. The arrowed lines represent the formation rates of the species they point to, the full green lines are for formation rates over 10^{17} $cm^{-3}s^{-1}$, orange dashed lines are for formation rates between 10^{17} and 10^{16} $cm^{-3}s^{-1}$, and red dotted lines are for formation rates between 10^{16} and 10^{15} $cm^{-3}s^{-1}$.

Starting from CO_2, the main reactions are electron impact dissociation towards CO and O [Reaction (6)] and electron impact ionization towards CO_2^+ [Reaction (20)]. Once ionization takes place, the main reaction path becomes $CO_2^+ + CO_2 + M \rightarrow C_2O_4^+ + M$ [Reaction (21)]. The $C_2O_4^+$ ions are further converted into $C_2O_3^+$ and $C_2O_2^+$ ions [Reactions (22) and (23)], and the latter ions split into two CO molecules or into CO and CO^+ [Reactions (24) and (25)]. The CO molecules are mainly consumed in these ion conversion processes, which again forms CO_2. Thus, a circular pathway interaction between CO and CO_2 takes place, as illustrated by Reactions (20)–(26), with no net conversion. The only net conversion [Reaction (27)] is due to electron impact dissociation [Reaction (6)]. This can be summarized as follows:

$$e^- + CO_2 \rightarrow CO + O + e^- \quad (6)$$

$$e^- + CO_2 \rightarrow CO_2^+ + e^- + e^- \quad (20)$$

$$2 \times (CO_2^+ + CO_2 + M \rightarrow C_2O_4^+ + M) \quad (21)$$

$$2 \times (C_2O_4^+ + CO + M \rightarrow C_2O_3^+ + CO_2 + M) \quad (22)$$

$$2 \times (C_2O_3^+ + CO + M \rightarrow C_2O_2^+ + CO_2 + M) \quad (23)$$

$$e^- + C_2O_2^+ \rightarrow CO + CO \quad (24)$$

$$C_2O_2^+ + M \rightarrow CO + CO^+ + M \quad (25)$$

$$CO^+ + CO_2 \rightarrow CO + CO_2^+ \quad (26)$$

Overall reaction:

$$3\,e^- + CO_2 \rightarrow CO + O + 3\,e^- \quad (27)$$

Furthermore, the O atoms formed by CO_2 splitting are also involved in a triangular interaction with O_2 and O_3, as already described in our earlier work,[28,69] and the main product is O_2. Thus, the two main products of CO_2 splitting are CO and O_2.

The interaction between CO_2 and H_2O takes place through the intermediate water products (H, OH, and HO_2) with O, O_2, O_3, and CO through the following main reactions [Eqs. (9), (28), (17), (8), (10), (29)]:

$$H + O_2 + M \rightarrow HO_2 + M \quad (9)$$

$$H + O_3 \rightarrow OH + O_2 \quad (28)$$

$$OH + O \rightarrow H + O_2 \quad (17)$$

$$OH + CO \rightarrow H + CO_2 \quad (8)$$

$$HO_2 + O \rightarrow O_2 + OH \quad (10)$$

$$HO_2 + OH \rightarrow H_2O + O_2 \quad (29)$$

Starting from H_2O the main reaction is also electron impact dissociation into OH and H [see Reaction (7)]. Other products formed are H_2 [mainly through Reactions (30) and (31)] and intermediate ions such as H_3O^+ (not included in the reactions). Although the formation rates of H_2 are only moderate, its loss rates are even lower, which explains why it is still one of the main reaction products. Finally, OH^- and H recombine to H_2O with the release of an electron, and again 2 OH radicals can react with each other in the presence of a third body to form H_2O_2 [Reactions (32) and (15)]. The main reaction for OH and H radicals, generated from Reaction (7), is their recombination

into H_2O [see Reaction (11)]. Moreover, part of the OH radicals also recombine into H_2O_2 through a third body reaction [see Reaction (15)]. This reaction is indeed the main production pathway for hydrogen peroxide, as explained above. In turn, H_2O_2 can be destroyed upon reaction with an additional OH radical [see Reaction (34)]. Just like for O, O_2, and O_3, an interaction takes place between OH, HO_2, and H_2O_2, which can be summarized as follows: HO_2, mainly formed from H and O_2 [Reaction (9)], reacts with O to form OH [Reaction (10)]. As explained above, HO_2 can also recombine to form H_2O_2 [Reaction (18)] and again part of this H_2O_2 is converted back into HO_2 [Reaction (34)] which goes on to produce O_2 [Reaction (10).

If we combine the net Reactions (33) and (35), we get the overall Reaction (36), which is one of the most important reaction paths for the conversion of CO_2 and H_2O in the main observed products O_2, CO, H_2, and H_2O_2.

$$e^- + H_2O \rightarrow OH + H + e^- \quad (7)$$

$$e^- + H_2O \rightarrow OH + H^- \quad (30)$$

$$H^- + H_2O \rightarrow OH^- + H_2 \quad (31)$$

$$H + OH^- \rightarrow H_2O + e^- \quad (32)$$

$$OH + OH + M \rightarrow H_2O_2 + M \quad (15)$$

Net reaction:

$$2\,e^- + 2\,H_2O \rightarrow H_2 + H_2O_2 + 2\,e^- \quad (33)$$

$$2 \times (e^- + CO_2 \rightarrow CO + O + e^-) \quad (6)$$

$$3 \times (e^- + H_2O \rightarrow OH + H + e^-) \quad (7)$$

$$OH + H + M \rightarrow H_2O + M \quad (11)$$

$$OH + OH + M \rightarrow H_2O_2 + M \quad (15)$$

$$H_2O_2 + OH \rightarrow H_2O + HO_2 \quad (34)$$

$$2 \times (H + O_2 + M \rightarrow HO_2 + M) \quad (9)$$

$$HO_2 + O \rightarrow OH + O_2 \quad (10)$$

$$HO_2 + HO_2 + M \rightarrow H_2O_2 + O_2 + M \quad (18)$$

$$H_2O_2 + OH \rightarrow H_2O + HO_2 \quad (34)$$

$$HO_2 + O \rightarrow OH + O_2 \quad (10)$$

Net reaction:

$$2\,e^- + 2\,CO_2 \rightarrow 2\,CO + O_2 + 2\,e^- \quad (35)$$

Overall reaction:

$$4\,e^- + 2\,H_2O + 2\,CO_2 \rightarrow 2\,CO + O_2 + H_2 + H_2O_2 + 4\,e^- \quad (36)$$

Model predictions in a wider range

So far our experiments and modeling calculations are perfectly in line with four of the five main observations from the literature (see end of the state-of-the-art section): one, CO_2 conversion increases with increasing energy input; two, CO_2 conversion drops with increasing water content; three, the H_2/CO ratio increases with increasing water content; four, the main products formed are H_2, CO, O_2, and (parts-per-million amounts of) H_2O_2.

Nevertheless, the above study could only be performed for a small range of experimental conditions on the basis of the available set up. To analyze this process for a wider range of conditions and especially to reveal whether the latter could yield certain products in larger amounts, we performed additional model calculations beyond what is typically accessible for one experimental setup. More specifically, we varied the SEI from 5 to 250 J cm^{-3} for water contents from 10 to 90%.

Given that this newly developed chemistry model was not validated in this wider range of conditions, caution is advised with its interpretation and predictive value. Another critical note is that the experimental conditions required to achieve the highest water contents under study might not be straightforward to realize owing to the condensation issues already observed at low concentrations. One solution might, therefore, be to dilute the entire mixture with an inert gas, such as argon or helium. Nitrogen is probably less suited, as it gives rise to NO_x formation.[69] This approach would also solve possible safety issues but, on the other hand, increase the energy cost, as discussed in the summary section below.

Although caution is advised in extrapolating models outside their validated range, our previous modeling studies[14,28,62,69,73] for several different mixtures have already shown that, in general, the plasma chemistry behavior is almost independent of the SEI, which shows a steadily increasing trend in conversion and production. The same studies with admixtures have also shown that, in general, plasma chemistry follows a stable and logic trend upon changing the mixture ratios. Furthermore, we performed a sensitivity analysis for the most important reactions, which showed that by taking the uncertainties of the reaction rate constants into account, the average deviation on the calculation results is indeed independent of the SEI and only approximately 2% on average (see the Supporting Information for more details). Hence, extrapolation of the model to a wider range of conditions would give us the opportunity to investigate whether the same results could be expected in this wider range and/or whether certain products could be formed in larger amounts and, thus, would give an indication whether it would be worth pursuing these other conditions experimentally. Below, the obtained results will be briefly summarized, but more details can be found in the Supporting Information.

The absolute CO_2 conversion (see Figure S7a) shows the same trends as those observed before: it increases with increasing SEI, and it drops with increasing water content over the entire range, and the initial drop is the most pronounced. The absolute H_2O conversion, on the other hand, shows different trends depending on the SEI, that is, it either drops or rises

with increasing water content at low or high SEI values (see Figure S7 b). Furthermore, at low water contents, it now drops with increasing SEI. This clearly indicates that the CO_2 chemistry shows mainly the same behavior as that presented above, whereas the H_2O chemistry changes with increasing SEI and water content.

The main products are again O_2 and the syngas components CO and H_2, whereas the oxygenated hydrocarbons are again not formed in concentrations above 20 ppm. However, the production of H_2O_2 increases significantly upon increasing the SEI and water content, and concentrations in the range of 300 ppm to 2.2% are achieved (see Tables in Section S2.2.2.). Upon increasing the water content the same logical trends as those in Table 1 are also observed, that is, a drop in the O_2, CO, and O_3 concentrations and an increase in the H_2 and H_2O_2 concentrations. The H_2 concentration increases significantly upon the addition of more water and becomes clearly larger than the concentration of CO for the highest water contents. This has a beneficial effect for the H_2/CO ratio, which increases drastically with the water content (see Figure S9). Moreover, it drops upon increasing the SEI, which is in line with the fifth observation reported in the literature.[15,59] The latter can be explained by the effective H_2O conversion, which starts to saturate with increasing SEI, whereas the effective CO_2 conversion keeps on rising. The maximum calculated H_2/CO ratio is approximately 8.6 and is obtained at 5 J cm^{-3} with a water content of 90% (see Figure S9). As such, our earlier claim that plasma technology allows for a process with a controllable H_2/CO ratio is confirmed in this wider range of water contents and SEI values. Our calculations reveal that depending on the water content and SEI, a CO_2/H_2O plasma is able to supply a hydrogen-rich syngas ratio for both various direct Fischer–Tropsch synthesis processes and methanol synthesis.

The chemical behavior in this extended range can be explained with Figure 5. CO_2 is split into CO and O, which will subsequently form O_2, and there is no "fast" pathway back to CO_2. H_2O, on the other hand, is split into OH and H, both of which are reactive products, and the "fastest" pathway for both is recombination back to H_2O. Hence, owing to Le Chatelier's principle, upon increasing the SEI, the CO_2 conversion will keep on rising, as its dissociation products (i.e., O) react away or are stable molecules (i.e., O_2 and O_3) that do not quickly react back to CO_2, whereas for H_2O, an equilibrium between conversion and formation will be reached, which explains why the H_2O conversion reaches a maximum or saturates at a certain SEI value. Even the production of H_2O_2 cannot prevent this, as it is also easily split into OH radicals, which again leads to the formation of H_2O.

Summary: Potential and limitations of CO_2/H_2O plasma conversion

From the above reaction schemes and chemical kinetics analysis, we can draw a number of conclusions. The bad news is that CO_2 and H_2O seem to be unsuitable to create methanol (or other oxygenated hydrocarbons) in a one-step process by means of a DBD plasma. There are too many steps involved in generating CH_3OH in an efficient way, and all of them involve H atoms, which will, in our case, more quickly recombine with OH into H_2O or with O_2 into HO_2, which also reacts further with O into OH. Consequently, we would need to inhibit these two reactions (i.e., both with OH and with O_2). However, even then, the H atoms would more quickly recombine with the O atoms into OH. The problem at hand is thus that the interactions of the H atoms with oxygen species (OH, O_3, O_2, or O atoms) are too fast and their tendency to form H_2O is too strong. This is of course not unexpected, as water is one of the end products of total combustion. Although this fast reaction between the H and O atoms has already been proven useful in other plasma-based applications (more specifically for O trapping in the case of CO_2 conversion, which provides a solution for the separation of the CO_2 splitting products),[74] here it plays against us.

On the other hand, our calculations do reveal that a CO_2/H_2O DBD plasma can deliver an easily controllable H_2/CO ratio with a rich hydrogen content if sufficient amounts of water can be added to the CO_2 plasma. Hence, at first sight it appears suitable to create value-added chemicals, including methanol, in a two-step process, which is good news. However, our calculations also show that the interactions between the H_2O and CO_2 dissociation products, that is, recombination between OH and CO into CO_2 and recombination of H and OH into H_2O, limit the CO_2 and H_2O conversions and, thus, the formation of useful products.

Besides syngas, the direct production of sufficient amounts of hydrogen peroxide, which can be used as a disinfectant or for biomedical purposes, seems possible. However, the formation rate of H_2O_2 is also partially limited by the destruction reaction of $OH + H_2O_2$ towards H_2O and HO_2. Therefore, again, rapid removal of the formed product (i.e., H_2O_2), for example, by means of a membrane, would be an important aspect for further improving this process.

On the basis of the reaction pathways outlined above, we believe that to produce value-added chemicals the plasma should be combined with a catalyst (so-called plasma catalysis).[63,75] This catalyst should selectively let the plasma-generated CO and H_2 react into methanol and subsequently separate the methanol generated from the mixture. For example, Eliasson et al.[72] used a CuO/ZnO/Al_2O_3 catalyst in a CO_2/H_2 discharge that led to an increase in methanol yield and selectivity by more than a factor 10. Several other reported catalysts used for the conversion of CO_2 with H_2 might also be interesting to investigate for their suitability in plasma catalysis, such as Ni-zeolite catalysts, for which methanation is reported,[76] a Rh_{10}/Se catalyst yielding an ethanol selectivity up to 83%,[77] and a Ni–Ga catalyst for conversion into methanol.[78] Furthermore, a lot of research into catalytic CO_2 hydrogenation is showing promising results for CuO/ZnO/ZrO_2, Cu/ZnO-based catalysts promoted with Pd and Ga, Pd/ZnO, and Pd/SiO_2 with the addition of Ga.[79] In general, multicomponent systems (Cu/ZnO/ZrO_2/Al_2O_3/SiO_2) have reported good performances for the formation of methanol starting from CO/CO_2/H_2 mixtures,[77] which makes them potentially very interesting for plasma catalysis, as this is the in situ generated mixture during

plasma-based conversion, as demonstrated in our paper. The additional advantage is that adding a catalyst should also enhance the conversions because of Le Chatelier's principle. However, it is important to realize that the catalyst affects the discharge and vice versa,[63,75] so it is recommended to use tailored catalysts for the plasma process rather than simply relying on classical catalysts. As stated by Neyts et al.[63] it is important to distinguish between physical and chemical effects if introducing a catalyst in a plasma. In this case, we are mainly interested in improving the selectivity towards targeted (value-added) products; therefore, the focus should mainly be on the chemical effects. This could be done by replacing the stainless steel inner electrode by another metal (e.g., Cu or Ni),[80] although care should be taken that the contact time between the plasma species and the catalyst is long enough. For this purpose, adding catalyst pellets in the entire reactor volume, such as in a packed-bed reactor, might be more suitable. Keeping in mind the reaction scheme and reactive species predicted by our model, two pathways might be interesting and realistic to achieve: promoting the recombination of OH radicals to H_2O_2 or promoting the reduction of CO to methanol. In both cases, the thermodynamic aspects at the nanoscale will become very important, especially because plasma catalysis is a far-from-equilibrium process.[75] The critical point will be the arrival and binding (e.g., physi- or chemisorption) of the reactants to the catalyst surface. To be successful, this process will have to be faster than the recombination rate of OH with H. Of course, these suggestions are only speculations, and further research will be needed to investigate this in practice.

Note, however, that we need to be cautious about the explosive mixture that might be formed during this process, owing to the presence of O_2, together with CO, H_2, and an ignition source in such a setup. At the research level, this will probably never be a problem because of the low volumes and conversions. However, upon going to a pilot or industrial scale, with larger volumes and conversions, the risk will increase significantly. Consequently, both the capital and operating costs will increase drastically to ensure safe operations. One way to circumvent this problem is by diluting this mixture with an inert gas, such as argon or helium. In this case, however, additional separation (for the products) and recuperation (for the inert gas) steps will need to be included, which will also increase the cost. Furthermore, part of the input energy will be lost as a result of the electron impact excitation and ionization of these gases. Therefore, this will reduce the energy efficiency and increase the operating cost, but it ensures safe operations.

Finally, the energy efficiency in a classical DBD reactor is quite limited, that is, in the order of a maximum of 10% for pure CO_2 splitting,[28] and it will be even lower in the CO_2/H_2O mixture owing to the lower conversion, as indicated in this paper. This again limits the industrial applicability of CO_2/H_2O conversion in a DBD reactor. On the other hand, different plasma reactors, such as microwave or gliding arc plasmas, are characterized by higher energy efficiencies, that is, in the order of 50%, because of the importance of the vibrational kinetics of CO_2 under these conditions.[33,51] Moreover, they operate at somewhat higher temperatures, that is, in the order of 1000 K, which enables the addition of more H_2O. Nevertheless, it has been suggested[35,36] that H_2O might quench the vibrational levels of CO_2, which would thus reduce the good energy efficiency characteristic for these types of plasma reactors.

Conclusions

The purpose of this work was to evaluate the viability of plasma technology for the combined conversions of CO_2 and H_2O into value-added products by obtaining a better understanding of plasma chemistry on the basis of a combined experimental and computational study. First, a novel plasma chemistry set was developed on the basis of available data in the literature. More importantly, this model was then used to identify and analyze the underlying plasma chemical kinetic behavior, and this allowed us to evaluate whether the combined conversions of CO_2 and H_2O by using plasma could become a viable route to produce value-added chemicals. We focused on the effects of the water content and specific energy input (SEI) on the conversions of H_2O and CO_2 as well as on the formation of products, such as H_2, CO, O_2, H_2O_2, and oxygenated hydrocarbons (i.e., methanol).

We demonstrated that adding a small percentage of water to a CO_2 plasma in a dielectric barrier discharge (DBD) led to a steep drop in the CO_2 conversion, and upon adding even more water, the conversions of both CO_2 and H_2O kept decreasing slightly. Furthermore, as also observed in pure CO_2 and CO_2/CH_4 or CO_2/N_2 mixtures, the conversions of both CO_2 and H_2O increased upon increasing the SEI, which resulted from a lower flow rate (or higher residence time) or a higher power. The main products formed were CO, H_2, and O_2, as well as up to 2% H_2O_2 for high SEI values and water contents.

A detailed kinetic analysis by our model indeed revealed the following: one, why the CO_2 conversion decreases upon adding water; two, why the H_2O conversion is limited; three, why no methanol (or other oxygenated hydrocarbons) formation is observed; four, how H_2O_2 is formed. In general, the main reactive species created in the plasma were found to be OH, CO, O, and H. The OH radicals will quickly recombine with CO into CO_2, which thereby limits the CO_2 conversion upon the addition of water, whereas the O and H atoms will undergo reactions to form H_2O again, and this explains why the H_2O conversion is also limited. Furthermore, the fast reaction between O/OH and the H atoms also explains why no oxygenated products are formed, because it occurs much faster than the possible pathways that might lead to oxygenates.

Given that we could elucidate the underlying mechanisms of the limited conversions of CO_2 and H_2O and the absence of methanol formation on the basis of our kinetic analysis, this allowed us to look for possible solutions to overcome these limitations. However, owing to its inherent nature, this mixture seems unsuitable to produce methanol directly in a one-step process by using a DBD plasma, unless a suitable catalyst can be found. Furthermore, although plasma technology would allow for a process with an easily steerable syngas ratio—even up to 8.6 according to the extended calculations—making it suitable for Fischer–Tropsch synthesis and a two-step process

for methanol synthesis, the presence of a highly flammable/explosive mixture makes it doubtful that plasma technology will be the most suitable process for the combined conversions of CO_2 and H_2O on a large industrial scale. One way to solve this problem would be to dilute the gas mixture with an inert gas, such as argon or helium. The downside, however, is that part of the energy input would be lost to excite and ionize these gases, and an additional separation and recuperation step would need to be added, which would thus lead to a significant drop in the overall energy efficiency.

Experimental Section

Experimental studies

The experiments are performed in a coaxial DBD reactor (see Figure 6). A stainless steel mesh (ground electrode) was wrapped

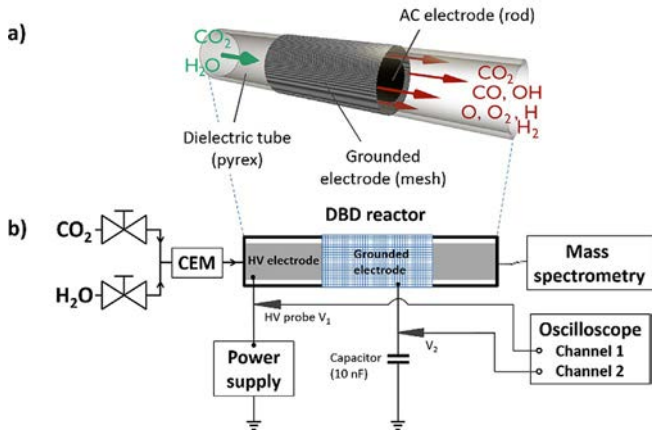

Figure 6. Depiction of a) the experimental DBD reactor and b) the experimental setup.

over the outside of a borosilicate (Pyrex) tube with outer and inner diameters of 30 and 26 mm, respectively (dielectric thickness = 2 mm). A copper rod with a diameter of 22 mm was placed in the center of the borosilicate tube and was used as a high-voltage electrode. The length of the discharge region was 100 mm with a discharge gap of 2 mm, which gave rise to a discharge volume of 15.1 cm^3. The DBD was supplied with an AFS generator G10S-V for a maximum power of 1000 W, with a maximum peak-to-peak voltage of 5 kV and a frequency of 28.06 kHz. The Q-U Lissajous method[28,81] was used to calculate the discharge power. The energy input was defined as the specific energy input (SEI), which is equal to the ratio of the calculated discharge power to the gas flow rate [Eq. (37)]:

$$\mathrm{SEI}\ [\mathrm{J\,cm^{-3}}] = \frac{\text{discharge power}\ [\mathrm{W}]}{\text{flow rate}\ [\mathrm{mL\,min^{-1}}]} \cdot \frac{60\ [\mathrm{s\,min^{-1}}]}{1\ [\mathrm{cm^3\,mL^{-1}}]} \quad (37)$$

Note that the SEI is used here as a parameter for energy input. Normally, it is rather the energy selectivity that is most important, as it defines the fraction of input energy used to drive the reactions compared to the energy lost to heating. However, in a DBD there is only local heating due to the discharge filaments. The latter only accounts for a very small fraction of the reactor volume for several nanoseconds, with a repetition in the microseconds scale, which yields a volume-corrected filament frequency of approximately 0.01 % per discharge cycle.[82] Thus, overall the gas heating is very limited, and we can assume that all the energy, as defined by the SEI, goes into driving the reactions. Of course, there are energy losses upon converting the (low voltage) outlet power to (high voltage) applied power to discharge power. To date, those may vary greatly depending on the power supply used, but this is independent from the plasma process under study. As such, a lot of (successful) research progress is still being made in minimizing the electrical conversion from outlet power to discharge power.

CO_2 and water vapor were used as feed gases with a continuous total flow rate of 600 mL min^{-1} at 323 K, varying the H_2O content in the mixture between 0 and 8 %, which resulted in a CO_2 content between 100 and 92 %. The individual CO_2 and water flow rates were controlled by a mass flow controller (Bronkhorst) and a liquid flow controller (Bronkhorst), respectively. Subsequently, both flows were mixed by using a controlled evaporator mixer (CEM, Bronkhorst), in which both the liquid and the gas flow were heated up in a controlled manner for total evaporation. Finally, this liquid delivery system with vapor control was connected to the DBD reactor. Additionally, the entire system (tubing and reactor) was heated up to 323 K to minimize condensation and to promote total evaporation of the water throughout the discharge, as much as possible.

The CO_2 and H_2O conversions were studied by mass spectrometry operating at atmospheric pressure (Hiden Analytical QGA MS, Warrington, UK). The multilevel software package MASsoft7 Professional was used, which allowed simple control of the mass spectrometer parameters. This software also permitted the electron energy in the ionization chamber to be set at 35 eV or lower for soft ionization for complex mixtures to have a reduced spectral fragmentation and simplified data interpretation, for example, in the case of the presence of more than one reactive component in the discharge. In our case, the electron energy in the ionization chamber was set at 35 eV, the detector was a secondary electron multiplier (SEM), and the MASsoft7 software was used to simultaneously monitor the partial pressure variations with specific m/z ratios as a function of time. The electrical measurements were performed by means of an oscilloscope (Tektronix DPO 3032) and a high-voltage probe (Tektronix P6015A) to evaluate the properties of the discharge. As indicated in Figure 6, the potential V_2 was measured through a capacitor of 10 nF (placed in series with the DBD) to evaluate the power absorbed by the plasma (P_{abs}) by the Lissajous method. This power was used as input in our simulations. Each experiment was repeated three times and the standard deviation was used to express the experimental uncertainties for the presented results. For more details, see the Supporting Information.

The absolute conversion, X_{abs}, of CO_2 and H_2O was calculated from the mass spectrometry response [Eqs. (38) and (39)]:

$$X_{\mathrm{abs,\ CO_2}} = \frac{\dot{n}_{\mathrm{CO_2,inlet}} - \dot{n}_{\mathrm{CO_2,outlet}}}{\dot{n}_{\mathrm{CO_2,inlet}}} \quad (38)$$

$$X_{\mathrm{abs,\ H_2O}} = \frac{\dot{n}_{\mathrm{H_2O,inlet}} - \dot{n}_{\mathrm{H_2O,outlet}}}{\dot{n}_{\mathrm{H_2O,inlet}}} \quad (39)$$

in which $\dot{n}_i$ is the molar flow rate of species i.

The effective conversion, X_{eff}, was obtained by multiplying the absolute conversion, X_{abs}, with the relative gas content [Eqs. (40) and

(41)]:

$$X_{\mathrm{eff},CO_2} = X_{\mathrm{abs},CO_2} \cdot \frac{\dot{n}_{CO_2,\mathrm{inlet}}}{\dot{n}_{CO_2,\mathrm{inlet}} + \dot{n}_{H_2O,\mathrm{inlet}}} \quad (40)$$

$$X_{\mathrm{eff},H_2O} = X_{\mathrm{abs},\,H_2O} \cdot \frac{\dot{n}_{H_2O,\mathrm{inlet}}}{\dot{n}_{CO_2,\mathrm{inlet}} + \dot{n}_{H_2O,\mathrm{inlet}}} \quad (41)$$

We defined here the effective conversion, along with the absolute conversion, because in plasma research the gas under study is often diluted by helium, argon, or nitrogen. Owing to this dilution and some energy-transfer processes that might occur (e.g., Penning ionization and dissociation), the absolute conversion might increase significantly. However, (a large) part of the input energy is also lost to this dilutant. Therefore, to allow for easier comparison between diluted and undiluted results, both the absolute and effective conversion are important.

To analyze the products, two different selectivities were defined, that is, the O-based selectivity for the O-containing species (e.g., O_2, CO, and H_2O_2) and the H-based selectivity for the H-containing species (e.g., H_2 and H_2O_2).

O-based selectivity [Eqs. (42)–(44)]:

$$S_{O,CO} = \frac{\dot{n}_{CO,\mathrm{out}}}{2 \cdot \left[\left(\dot{n}_{CO_2,\mathrm{in}} - \dot{n}_{CO_2,\mathrm{out}}\right) + 1/2 \cdot \left(\dot{n}_{H_2O,\mathrm{in}} - \dot{n}_{H_2O,\mathrm{out}}\right)\right]} \quad (42)$$

$$S_{O,O_2} = \frac{\dot{n}_{O_2,\mathrm{out}}}{\left(\dot{n}_{CO_2,\mathrm{in}} - \dot{n}_{CO_2,\mathrm{out}}\right) + 1/2 \cdot \left(\dot{n}_{H_2O,\mathrm{in}} - \dot{n}_{H_2O,\mathrm{out}}\right)} \quad (43)$$

$$S_{O,H_2O_2} = \frac{\dot{n}_{H_2O_2,\mathrm{out}}}{\left(\dot{n}_{CO_2,\mathrm{in}} - \dot{n}_{CO_2,\mathrm{out}}\right) + 1/2 \cdot \left(\dot{n}_{H_2O,\mathrm{in}} - \dot{n}_{H_2O,\mathrm{out}}\right)} \quad (44)$$

H-based selectivity [Eqs. (45) and (46)]:

$$S_{H,H_2} = \frac{\dot{n}_{H_2,\mathrm{out}}}{\left(\dot{n}_{H_2O,\mathrm{in}} - \dot{n}_{H_2O,\mathrm{out}}\right)} \quad (45)$$

$$S_{H,H_2O_2} = \frac{\dot{n}_{H_2O_2,\mathrm{out}}}{\left(\dot{n}_{H_2O,\mathrm{in}} - \dot{n}_{H_2O,\mathrm{out}}\right)} \quad (46)$$

Computational studies

0D chemical kinetics model

The plasma chemistry set developed in this work was applied to a zero-dimensional (0D) kinetic model, called Global_kin, developed by Kushner and co-workers[83,84] to describe the underlying reactions taking place. The time-evolution of the species densities was calculated on the basis of production and loss processes, as defined by the chemical reactions. The rate coefficients of the heavy particle reactions depended on the gas temperature and were calculated by Arrhenius equations. The rate coefficients for the electron impact reactions were a function of the electron temperature and were calculated in the Boltzmann equation module. Finally, the electron temperature was calculated with an energy balance equation. More details about this model can be found in the work of Kushner et al.[83,84] and in the Supporting Information.

Plasma chemistry included in the model

The data to compile the necessary plasma chemistry was taken from different sources and was expanded with additional CO_2/H_2O interactions. For example, the CO_2 chemistry and the H_2O/O_2 chemistry used in this study were mainly adopted from Aerts et al.[85] and van Gaens et al.,[86] respectively. The hydrocarbon chemistry, necessary to describe the reactions between the CO_2 and H_2O species and, thus, for product formation, was partially taken from Snoeckx et al.[62] The total chemistry set considered 75 different species (listed in Table 3), which reacted with each other in 187 electron impact reactions, 346 ion reactions, and 369 neutral reactions. Their corresponding rate coefficients and the references from which these data were adopted are listed in Refs. [62,85,86] and can be found in the Supporting Information.

Table 3. Species included in the model.

Species	Examples
C–O	CO_2, CO, C_2O, CO_2^+, CO^+, CO_4^+, CO_4^-, CO_3^-, $C_2O_4^+$, $C_2O_3^+$, $C_2O_2^+$
C	C, C_2, C_2^+, C^+
O	O_3, O_2, O, O_4^-, O_3^-, O_2^-, O^-, O_4^+, O_2^+, O^+
C–H	CH_4, CH_3, CH_2, CH, CH_5^+, CH_4^+, CH_3^+, CH_2^+, CH^+
C_2–H	C_2H_6, C_2H_5, C_2H_4, C_2H_3, C_2H_2, C_2H, $C_2H_6^+$, $C_2H_5^+$, $C_2H_4^+$, $C_2H_3^+$, $C_2H_2^+$
$C_{3/4}$–H	C_3H_8, C_3H_7, C_3H_6, C_4H_2
H	H_2, H, H_3^+, H_2^+, H^+, H^-
H–O	H_2O, OH, HO_2, H_2O_2, OH^-, H_3O^+, H_2O^+, OH^+
C–H–O	CHO, CH_2O, CH_3O, CH_2OH, CH_3OH, CHCO, CH_2CO, CH_3CO, CH_2CHO, CH_3CHO, $C_2H_5O_2$
electrons	e^-

From Table 2 it is evident that several high-value oxygenates, such as oxalic acid, formic acid, DME, and ethanol, were not included in our model, because of the lack of complete data on the specific reaction rate coefficients in the literature needed to describe their formation and loss processes. Of course, we could have incorporated these species, but because of the scarcity of coherent input data, their densities would be subject to such large uncertainties that the predictive character of the model would have less to no value. Furthermore, these oxygenates were not detected in our experiments. In the literature, some of them were detected, but this was in a microwave plasma setup, which operated under significantly different conditions than those of the DBD plasma under study here. Last, but not least, as will be illustrated in the chemical analysis section, the oxygenates that were included in the model, such as methanol and formaldehyde, were barely formed (not in the calculations, nor in the experiments), and as the other high-value oxygenates (not included in the model) are likely to be formed from the same precursors, one can expect their formation to be of minor importance under the plasma conditions under study, as also supported by their experimental absence. Nevertheless, we hope that rate coefficients for these molecules will become available in the literature in the near future, which would allow us to build an even more complete model and, more importantly, to investigate under which other circumstances these oxygenates might be formed.

Additionally, one could wonder whether it is necessary to keep pursuing hundreds of reactions—with their specific coefficients

and so on—to perfect chemical kinetics chemistry models. In the section "Underlying mechanisms for the observed trends", it was possible to identify 23 different reactions for which a reaction scheme could be compiled and the observed trends explained. This is of course a big difference compared to the 902 different reactions that were included in the model. As such, one could indeed wonder about the necessity of including all these reactions. However, it is important to realize this information is evidently only available after the fact, and during the construction of these chemistry sets, missing one (seemingly unimportant) reaction can lead to dramatically wrong outcomes. Therefore, it is absolutely necessary to build a comprehensive set first. Furthermore, building a more complete chemistry set allows this set to be used to model different reactor types and conditions, as was done in this work for the extended range of H_2O concentrations and energy inputs. However, if a relatively complete chemistry model is available in the literature (as developed in this work) and one wants to optimize a specific setup and/or start modeling in two or three dimensions (to include geometry variations for example), from that point on it is of no use to continue pursuing a complete-as-possible model and one should focus on simplifying the chemistry to its bare essence. The latter is necessary not only to make the interpretation of the results easier to grasp but also because of computational restraints, as it is impossible to model a reactor in 3D with hundreds of reactions.

Sensitivity analysis of the rate coefficients

Given that most of the available reaction rate coefficients in the literature are prone to some deviations, we performed a sensitivity analysis for the most important reactions to give an additional indication of the reliability of the model and the predictive value of the model results and its uncertainties. Typically, the electron impact reaction rate constants calculated by using the two-term Boltzmann equation showed an uncertainty of approximately 30%, whereas the uncertainty on the rate constants of the most important heavy particle reactions was typically up to 100%. Therefore, we focused on the most important heavy particle reactions for this sensitivity analysis, more specifically those reactions that played a role in the important reaction paths; see the section on "Underlying mechanisms for the observed trends". From this analysis, we concluded that overall the uncertainties in the rate constants did not cause large deviations in the CO_2 and H_2O conversions, because a variation in the rate constants by 100% yielded only deviations in the calculation results in the order of at maximum 10%, and typically even lower than 5%. For more details about this sensitivity analysis see the Supporting Information.

Application of the 0D model to a DBD reactor

0D models can only calculate species densities as a function of time, and thus, they neglect spatial variations. Nevertheless, by using the gas flow rate, the time evolution could be translated into a spatial evolution (i.e., as a function of position in the DBD reactor). This spatial evolution was necessary to mimic the typical filamentary behavior found in DBDs used for CO_2 conversion.[87] On their way throughout the reactor, the gas molecules will pass through several microdischarge filaments. This was mimicked in the model by applying a large number of consecutive triangular microdischarge pulses in the same way as that described in our previous work.[62] This approach was already proven to be applicable for a variety of conditions, gas mixtures, and different 0D simulation codes.[14,33,62,69,73,74,88] The experimental gas flow rate was used, that is, 600 mL min^{-1} at 323 K and atmospheric pressure, with a DBD reactor volume of 15.1 cm^3 (see above), which thus corresponded to a residence time of 1.66 s.

The model was run at a constant temperature of 323 K. In reality, the temperature might change as a result of the chemical reactions taking place (either exo- or endotherm). Indeed, a considerable fraction of the energy delivered to the plasma will be lost in reaction pathways that eventually lead to the reformation of the reactants [see Reactions (6)–(12)], and consequently, the energy supplied by the electrons to the chemical species will eventually be transformed into other forms of energy (e.g., thermal energy). This energy might lead to a local rise in the temperature, probably limited to the microdischarge volume, which might affect the chemical reactivity of the system. However, we believe that our assumption of constant temperature is in first instance justified, for the following reasons: one, there are both exothermic and endothermic reactions in the overall reaction chemistry, and the energy released by the exothermic reactions will be balanced by the endothermic reactions; two, in similar work on the dry reforming of methane[42,62] it was demonstrated that the conversion was mainly determined by the (gas-temperature-independent) electron impact reactions during (and shortly after) the microdischarge filaments, whereas most of the product formation (and hence the selectivities) was determined by the afterglow reactions. Furthermore, it was observed during temperature-controlled experiments that the conversions and selectivity did not change significantly upon increasing the temperature from 297 to 473 K.[42] Nevertheless, to check the validity of the assumption of constant temperature, we ran our model at two additional temperatures, that is, 373 and 423 K (instead of the standard calculations of 323 K). At 373 K, the relative changes in CO_2 conversion compared to the standard calculations were approximately +2–4%, and the relative changes in the H_2O conversion were approximately +2%. At 423 K, the relative changes in CO_2 conversion compared to the standard calculations were approximately +6–10%, and the relative changes in the H_2O conversion were approximately −10–13%. The selectivities remained almost unchanged, with only a significant +20–30% increase in the O_3 and H_2O_2 concentrations. However, we believe that such heating of the gas temperature in the reactor up to 423 K does not occur, as it was not observed experimentally, mainly owing to the small microdischarge volumes and the cooling as a result of the continuous gas flow.

Acknowledgements

The authors acknowledge financial support from the Inter-university Attraction Pole (IAP; grant number IAP-VII/12, P7/34) program "PSI-Physical Chemistry of Plasma-Surface Interactions", financially supported by the Belgian Federal Office for Science Policy (BELSPO), as well as the Fund for Scientific Research Flanders (FWO; grant number G.0066.12N). This work was performed in part using the Turing HPC infrastructure at the CalcUA core facility of the Universiteit Antwerpen, a division of the Flemish Supercomputer Center VSC, funded by the Hercules Foundation, the Flemish Government (department EWI) and the University of Antwerp. We also would like to thank the financial support given by "Fonds David et Alice Van Buuren". Finally, we are very grateful to M. Kushner for providing the Global kin code, to T. Dufour for his support during the experiments, and to R. Aerts for his support during the model development.

Keywords: carbon dioxide · kinetics · nonthermal plasma · plasma chemistry · water splitting

[1] R. K. Pachauri, L. A. Meyer, *IPCC, 2014: Climate Change 2014: Synthesis Report. Contribution of Working Groups I, II and III to the Fifth Assessment Report of the Intergovernmental Panel on Climate Change*, Geneva, Switzerland, **2014**.
[2] J. Albo, M. Alvarez-Guerra, P. Castaño, A. Irabien, *Green Chem.* **2015**, *17*, 2304 – 2324.
[3] G. Fiorani, W. Guo, A. W. Kleij, *Green Chem.* **2015**, *17*, 1375 – 1389.
[4] W. McDonough, M. Braungart, P. Anastas, J. Zimmerman, *Environ. Sci. Technol.* **2003**, *37*, 434A – 441A.
[5] J. Barber, *Chem. Soc. Rev.* **2009**, *38*, 185 – 196.
[6] E. E. Benson, C. P. Kubiak, A. J. Sathrum, J. M. Smieja, *Chem. Soc. Rev.* **2009**, *38*, 89 – 99.
[7] M. Aresta, A. Dibenedetto, A. Angelini, *Chem. Rev.* **2014**, *114*, 1709 – 1742.
[8] J. R. Scheffe, A. Steinfeld, *Mater. Today* **2014**, *17*, 341 – 348.
[9] E. V. Kondratenko, G. Mul, J. Baltrusaitis, G. O. Larrazabal, J. Perez-Ramirez, G. O. Larrazábal, J. Pérez-Ramírez, *Energy Environ. Sci.* **2013**, *6*, 3112 – 3135.
[10] A. H. McDaniel, E. C. Miller, D. Arifin, A. Ambrosini, E. N. Coker, R. O'Hayre, W. C. Chueh, J. Tong, *Energy Environ. Sci.* **2013**, *6*, 2424 – 2428.
[11] A. Goeppert, M. Czaun, J.-P. Jones, G. K. Surya Prakash, G. A. Olah, *Chem. Soc. Rev.* **2014**, *43*, 7995 – 8048.
[12] C. Liu, G. Xu, T. Wang, *Fuel Process. Technol.* **1999**, *58*, 119 – 134.
[13] S. Samukawa, M. Hori, S. Rauf, K. Tachibana, P. Bruggeman, G. Kroesen, J. C. Whitehead, A. B. Murphy, A. F. Gutsol, S. Starikovskaia, U. Kortshagen, J.-P. Boeuf, T. J. Sommerer, M. J. Kushner, U. Czarnetzki, N. Mason, *J. Phys. D: Appl. Phys.* **2012**, *45*, 253001.
[14] R. Snoeckx, Y. X. Zeng, X. Tu, A. Bogaerts, *RSC Adv.* **2015**, *5*, 29799 – 29808.
[15] G. Chen, T. Silva, V. Georgieva, T. Godfroid, N. Britun, R. Snyders, M. P. Delplancke-Ogletree, *Int. J. Hydrogen Energy* **2015**, *40*, 3789 – 3796.
[16] Z. Jiang, T. Xiao, V. L. Kuznetsov, P. P. Edwards, *Philos. Trans. R. Soc. London Ser. A* **2010**, *368*, 3343 – 3364.
[17] M. Mikkelsen, M. Jørgensen, F. C. Krebs, *Energy Environ. Sci.* **2010**, *3*, 43 – 81.
[18] G. Centi, E. A. Quadrelli, S. Perathoner, *Energy Environ. Sci.* **2013**, *6*, 1711 – 1731.
[19] P. L. Spath, D. C. Dayton, *Preliminary Screening — Technical and Economic Assessment of Synthesis Gas to Fuels and Chemicals with Emphasis on the Potential for Biomass-Derived Syngas*, **2003,** National Renewable Energy Laboratory, Golden, CO. handle.dtic.mil/100.2/ADA436529.
[20] E. Linley, S. P. Denyer, G. McDonnell, C. Simons, J. Y. Maillard, *J. Antimicrob. Chemother.* **2012**, *67*, 1589 – 1596.
[21] G. McDonnell in *New Biocides Development: The Combined Approach of Chemistry and Microbiology (ACS Symposium Series Vol. 967)* (Ed.: P. C. Zhu), American Chemical Society, Washington, D.C., **2007**, pp. 292 – 308
[22] M. Finnegan, E. Linley, S. P. Denyer, G. McDonnell, C. Simons, J. Y. Maillard, *J. Antimicrob. Chemother.* **2010**, *65*, 2108 – 2115.
[23] D. Dobyrin, G. Fridman, G. Friedman, A. Fridman, *New J. Phys.* **2009**, *11*, 115020.
[24] J. Ehlbeck, U. Schnabel, M. Polak, J. Winter, T. von Woedtke, R. Brandenburg, T. von dem Hagen, K.-D. Weltmann, *J. Phys. D: Appl. Phys.* **2011**, *44*, 013002.
[25] J. Winter, H. Tresp, M. U. Hammer, S. Iseni, S. Kupsch, A. Schmidt-Bleker, K. Wende, M. Dünnbier, K. Masur, K.-D. Weltmann, S. Reuter, *J. Phys. D: Appl. Phys.* **2014**, *47*, 285401.
[26] X. Lu, G. V. Naidis, M. Laroussi, S. Reuter, D. B. Graves, K. Ostrikov, *Phys. Rep.* **2016**, *630*, 1 – 84.
[27] A. Bogaerts, T. Kozák, K. van Laer, R. Snoeckx, *Faraday Discuss.* **2015**, *183*, 217 – 232.
[28] R. Aerts, W. Somers, A. Bogaerts, *ChemSusChem* **2015**, *8*, 702 – 716.
[29] S. Heijkers, R. Snoeckx, T. Kozák, T. Silva, T. Godfroid, N. Britun, R. Snyders, A. Bogaerts, *J. Phys. Chem. C* **2015**, *119*, 12815 – 12828.
[30] T. Silva, N. Britun, T. Godfroid, R. Snyders, *Plasma Sources Sci. Technol.* **2014**, *23*, 025009.
[31] A. P. H. Goede, W. A. Bongers, M. F. Graswinckel, R. M. C. M. Van De Sanden, M. Leins, J. Kopecki, A. Schulz, M. Walker, *EPJ Web Conf.* **2014**, *79*, 01005.
[32] F. Brehmer, S. Welzel, R. M. C. M. Van De Sanden, R. Engeln, *J. Appl. Phys.* **2014**, *116*, 123303.
[33] T. Kozák, A. Bogaerts, *Plasma Sources Sci. Technol.* **2014**, *23*, 045004.
[34] L. F. Spencer, A. D. Gallimore, *Plasma Sources Sci. Technol.* **2013**, *22*, 015019.
[35] A. Indarto, D. R. Yang, J.-W. Choi, H. Lee, H. K. Song, *J. Hazard. Mater.* **2007**, *146*, 309 – 315.
[36] T. Nunnally, K. Gutsol, A. Rabinovich, A. Fridman, A. Gutsol, A. Kemoun, *J. Phys. D: Appl. Phys.* **2011**, *44*, 274009.
[37] X. Tao, M. Bai, X. Li, H. Long, S. Shang, Y. Yin, X. Dai, *Prog. Energy Combust. Sci.* **2011**, *37*, 113 – 124.
[38] G. Petitpas, J. Rollier, A. Darmon, J. Gonzalez-Aguilar, R. Metkemeijer, L. Fulcheri, *Int. J. Hydrogen Energy* **2007**, *32*, 2848 – 2867.
[39] A. Janeco, N. R. Pinha, V. Guerra, *J. Phys. Chem. C* **2015**, *119*, 109 – 120.
[40] G. Scarduelli, G. Guella, D. Ascenzi, P. Tosi, *Plasma Processes Polym.* **2011**, *8*, 25 – 31.
[41] Y. Zhang, Y. Li, Y. Wang, C. Liu, B. Eliasson, *Fuel Process. Technol.* **2003**, *83*, 101 – 109.
[42] X. Zhang, M. S. Cha, *J. Phys. D: Appl. Phys.* **2013**, *46*, 415205.
[43] L. M. Martini, G. Dilecce, G. Guella, A. Maranzana, G. Tonachini, P. Tosi, *Chem. Phys. Lett.* **2014**, *593*, 55 – 60.
[44] D. Li, X. Li, M. Bai, X. Tao, S. Shang, X. Dai, Y. Yin, *Int. J. Hydrogen Energy* **2009**, *34*, 308 – 313.
[45] B. Eliasson, C. Liu, U. Kogelschatz, *Ind. Eng. Chem. Res.* **2000**, *39*, 1221 – 1227.
[46] V. J. Rico, J. L. Hueso, J. Cotrino, A. R. González-Elipe, *J. Phys. Chem. A* **2010**, *114*, 4009 – 4016.
[47] X. Tu, J. C. Whitehead, *Appl. Catal. B* **2012**, *125*, 439 – 448.
[48] Q. Wang, Y. Cheng, Y. Jin, *Catal. Today* **2009**, *148*, 275 – 282.
[49] B. Fidalgo, A. Domínguez, J. Pis, J. Menéndez, *Int. J. Hydrogen Energy* **2008**, *33*, 4337 – 4344.
[50] A. Ozkan, T. Dufour, G. Arnoult, P. De Keyzer, A. Bogaerts, F. Reniers, *J. CO_2 Util.* **2015**, *9*, 74 – 81.
[51] A. Fridman, *Plasma Chemistry*, Cambridge University Press, New York, **2008**.
[52] P. Bruggeman, C. Leys, *J. Phys. D: Appl. Phys.* **2009**, *42*, 053001.
[53] M. A. Malik, A. Ghaffar, S. A. Malik, *Plasma Sources Sci. Technol.* **2001**, *10*, 82 – 91.
[54] P. Sunka, V. Babický, M. Clupek, P. Lukes, M. Simek, J. Schmidt, M. Cernák, *Plasma Sources Sci. Technol.* **1999**, *8*, 258 – 265.
[55] B. R. Locke, S. M. Thagard, *Plasma Chem. Plasma Process.* **2012**, *32*, 875 – 917.
[56] T. Ihara, M. Kiboku, Y. Iriyama, *Bull. Chem. Soc. Jpn.* **1994**, *67*, 312 – 314.
[57] T. Ihara, T. Ouro, T. Ochiai, M. Kiboku, Y. Iriyama, *Bull. Chem. Soc. Jpn.* **1996**, *69*, 241 – 244.
[58] S. Futamura, H. Kabashima, *Stud. Surf. Sci. Catal.* **2004**, *153*, 119 – 124.
[59] S. Mahammadunnisa, E. L. Reddy, D. Ray, C. Subrahmanyam, J. C. Whitehead, *Int. J. Greenhouse Gas Control* **2013**, *16*, 361 – 363.
[60] N. Hayashi, T. Yamakawa, S. Baba, *Vacuum* **2006**, *80*, 1299 – 1304.
[61] L. Guo, X. Ma, Y. Xia, X. Xiang, X. Wu, *Fuel* **2015**, *158*, 843 – 847.
[62] R. Snoeckx, R. Aerts, X. Tu, A. Bogaerts, *J. Phys. Chem. C* **2013**, *117*, 4957 – 4970.
[63] E. C. Neyts, K. Ostrikov, M. K. Sunkara, A. Bogaerts, *Chem. Rev.* **2015**, *115*, 13408 – 13446.
[64] W. Bongers, H. Bouwmeester, B. Wolf, F. Peeters, S. Welzel, D. van den Bekerom, N. den Harder, A. Goede, M. Graswinckel, P. W. Groen, J. Kopecki, M. Leins, G. van Rooij, A. Schulz, M. Walker, R. van de Sanden, *Plasma Process. Polym.* **2016**, DOI: 10.1002/ppap.201600126.
[65] K. Van Laer, A. Bogaerts, *Plasma Sources Sci. Technol.* **2016**, *25*, 15002.
[66] Q. Yu, M. Kong, T. Liu, J. Fei, X. Zheng, *Plasma Chem. Plasma Process.* **2012**, *32*, 153 – 163.
[67] D. Mei, X. Zhu, Y.-L. He, J. D. Yan, X. Tu, *Plasma Sources Sci. Technol.* **2015**, *24*, 015011 – 015021.
[68] K. Van Laer, A. Bogaerts, *Energy Technol.* **2015**, *3*, 1038 – 1044.
[69] R. Snoeckx, S. Heijkers, K. Van Wesenbeeck, S. Lenaerts, A. Bogaerts, *Energy Environ. Sci.* **2016**, *9*, 999 – 1011.
[70] N. R. Pinhão, A. Janeco, J. B. Branco, *Plasma Chem. Plasma Process.* **2011**, *31*, 427 – 439.

[71] M. Ramakers, I. Michielsen, R. Aerts, V. Meynen, A. Bogaerts, *Plasma Processes Polym.* **2015**, *12*, 755 – 763.
[72] B. Eliasson, U. Kogelschatz, B. Xue, L.-M. Zhou, *Ind. Eng. Chem. Res.* **1998**, *37*, 3350 – 3357.
[73] R. Snoeckx, M. Setareh, R. Aerts, P. Simon, A. Maghari, A. Bogaerts, *Int. J. Hydrogen Energy* **2013**, *38*, 16098 – 16120.
[74] R. Aerts, R. Snoeckx, A. Bogaerts, *Plasma Processes Polym.* **2014**, *11*, 985 – 992.
[75] E. C. Neyts, K. Ostrikov, *Catal. Today* **2015**, *256*, 23 – 28.
[76] E. Jwa, S. B. Lee, H. W. Lee, Y. S. Mok, *Fuel Process. Technol.* **2013**, *108*, 89 – 93.
[77] G. Centi, S. Perathoner, *Catal. Today* **2009**, *148*, 191 – 205.
[78] F. Studt, I. Sharafutdinov, F. Abild-Pedersen, C. F. Elkjær, J. S. Hummelshøj, S. Dahl, I. Chorkendorff, J. K. Nørskov, *Nat. Chem.* **2014**, *6*, 320 – 324.
[79] S. G. Jadhav, P. D. Vaidya, B. M. Bhanage, J. B. Joshi, *Chem. Eng. Res. Des.* **2014**, *92*, 2557 – 2567.
[80] M. Scapinello, L. M. Martini, P. Tosi, *Plasma Processes Polym.* **2014**, *11*, 624 – 628.
[81] S. Paulussen, B. Verheyde, X. Tu, C. De Bie, T. Martens, D. Petrovic, A. Bogaerts, B. Sels, *Plasma Sources Sci. Technol.* **2010**, *19*, 34015.
[82] A. Bogaerts, W. Wang, A. Berthelot, V. Guerra, *Plasma Sources Sci. Technol.* **2016**, *25*, 55016.
[83] R. Dorai, M. J. Kushner, *J. Phys. D: Appl. Phys.* **2003**, *36*, 1075 – 1083.
[84] D. S. Stafford, M. J. Kushner, *J. Appl. Phys.* **2004**, *96*, 2451 – 2465.
[85] R. Aerts, T. Martens, A. Bogaerts, *J. Phys. Chem. C* **2012**, *116*, 23257 – 23273.
[86] W. Van Gaens, A. Bogaerts, *J. Phys. D: Appl. Phys.* **2013**, *46*, 275201.
[87] A. Ozkan, T. Dufour, T. Silva, N. Britun, R. Snyders, A. Bogaerts, F. Reniers, *Plasma Sources Sci. Technol.* **2016**, *25*, 025013.
[88] R. Aerts, X. Tu, W. Van Gaens, J. C. Whitehead, A. Bogaerts, *Environ. Sci. Technol.* **2013**, *47*, 6478 – 6485.

Manuscript received: September 5, 2016
Revised: October 13, 2016
Final Article published: November 25, 2016